

Mutual Inductance Sensing SQUID: Cryogenic microcalorimeter based on mutual inductance readout of superconducting temperature sensors

J. Zeuner,¹ C. Schuster,^{1, a)} and S. Kempf^{1, 2}

¹⁾*Institute of Micro- and Nanoelectronic Systems (IMS), Karlsruhe Institute of Technology (KIT), Hertzstrasse 16, Building 06.41, D-76187 Karlsruhe, Germany*

²⁾*Institute for Data Processing and Electronics (IPE), Karlsruhe Institute of Technology (KIT), Hermann-von-Helmholtz-Platz 1, Building 242, D-76344 Eggenstein-Leopoldshafen, Germany*

(*Electronic mail: sebastian.kempf@kit.edu)

(Dated: February 10, 2026)

Superconducting microcalorimeters, such as superconducting transition-edge sensors and magnetic microcalorimeters, have emerged as state-of-the-art detectors for x-ray emission spectroscopy by combining near-unity quantum efficiency with excellent energy resolution. Despite these achievements, their resolving power has not yet reached the level required to rival modern wavelength-dispersive grating or crystal spectrometers. Here, we introduce a next-generation SQUID-based microcalorimeter concept that exploits the strong temperature dependence of the magnetic penetration depth of a superconductor operated close to its critical temperature. The resulting mutual-inductance-based readout enables *in situ* tunable signal amplification, while inherently avoiding hysteretic effects that commonly limit superconducting sensors. Experiments with prototype devices demonstrate robust and reproducible operation over a wide temperature range. Based on our measurements and modeling, we project that an energy resolution below 100 meV should be achievable with an optimized absorber–sensor combination. This approach therefore represents a promising pathway towards next-generation cryogenic detectors for high-precision X-ray spectroscopy.

Cryogenic microcalorimeters have become indispensable tools for various applications, including X-ray emission spectroscopy at synchrotron light sources, ion-beam storage facilities or in laboratory environment^{1–4}. Established microcalorimeter concepts, such as superconducting transition-edge sensors (TESs)^{5,6} and magnetic microcalorimeters (MMCs)^{7–9}, have demonstrated exceptional performance and combine excellent energy resolution with near-unity quantum efficiency. They operate by detecting the minute temperature rise in an absorber following an X-ray absorption, which is converted into a measurable electrical signal by an ultrasensitive thermometer.

State-of-the-art TESs and MMCs achieve an energy resolution of ΔE_{FWHM} of 0.72 eV for 1.5 keV photons¹⁰ and 1.25 eV for 5.9 keV photons^{11,12}. In terms of resolving power, they thus approach the performance of wavelength-dispersive X-ray spectrometers, yet offer several orders of magnitude higher efficiency. However, despite these remarkable achievements, both TESs and MMCs face inherent challenges, including limited dynamic range, device fabrication complexity, stringent readout noise requirements, or sensor calibration constraints, which currently hinder their routine operation with sub-1 eV energy resolution. These limitations motivate the exploration of alternative detector concepts such as the Mutual Inductance Sensing SQUID (MISS) introduced in this work, alongside continued advancements in established detector technologies.

Figure 1 shows a simplified schematic circuit diagram of a Mutual Inductance Sensing SQUID (MISS), highlighting its key components. The central element is an ultrasen-

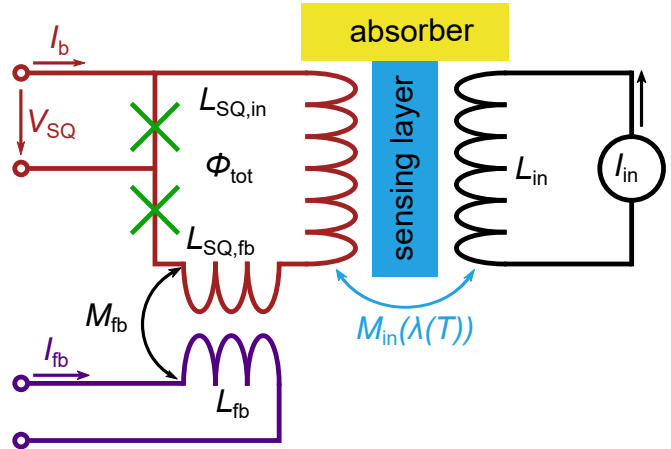


Figure 1. Schematic circuit diagram of a Mutual Inductance Sensing SQUID (MISS). The red-, black-, and purple-colored inductors are made from a superconducting material with critical temperature T_c . The sensing layer (blue) is made from a superconducting material with significantly lower critical temperature, i.e., $T_{c,\text{sens}} \ll T_c$, and is in good thermal contact with a suitable X-ray absorber. The device is operated at temperature $T_0 \lesssim T_{c,\text{sens}}$. A current source injects a constant current I_{in} into an input coil with inductance L_{in} . Owing to the temperature-dependent diamagnetic response of the sensing layer, the mutual inductance $M_{\text{in}}(\lambda(T))$ between the input coil and the inductively coupled SQUID loop segment with inductance $L_{\text{SQ,in}}$ becomes temperature dependent. The green crosses indicate resistively shunted Josephson tunnel junctions.

sitive thermometer that exploits the strong temperature dependence of the magnetic penetration depth of a superconducting thin film operated slightly below its transition temperature $T_{c,\text{sens}}$. The thermometer is sandwiched between a conventional direct-current superconducting quantum inter-

^{a)}Present address: Physikalisch-Technische Bundesanstalt (PTB) Braunschweig, Bundesallee 100, 38116 Braunschweig

ference device (dc-SQUID) and a superconducting input coil, both fabricated from a superconducting material with critical temperature $T_c \gg T_{c,\text{sens}}$. In addition, it is thermally coupled to a suitable particle absorber. The sensing layer is electrically floating, i.e., it has no galvanic contact with either the dc-SQUID or the input coil. Owing to its diamagnetic response, the superconducting sensing layer partially screens the SQUID loop from the magnetic flux generated by the input coil. As a consequence, the mutual inductance between the the input coil and the SQUID loop depends on the screening properties of the sensing layer. Since this screening is governed by the magnetic penetration depth $\lambda(T)$ of the sensing film, the mutual inductance becomes temperature dependent, i.e., $M_{\text{in}} = M_{\text{in}}(\lambda(T))$. By appropriate design of the sensing layer geometry and the choice of material, a very large temperature responsivity can be achieved, enabling the realization of highly sensitive microcalorimeters.

The dc-SQUID used for mutual inductance sensing consists of a superconducting loop with total inductance $L_{\text{SQ}} = L_{\text{SQ,in}} + L_{\text{SQ,fb}}$, which is interrupted by two Josephson tunnel junctions, each shunted by a resistor R . Magnetic flux is coupled into the SQUID loop either via the input coil with inductance L_{in} or via a feedback coil with inductance L_{fb} . The feedback coil enables flux-locked loop (FLL) SQUID operation as well as the application of a static flux bias for device characterization. The SQUID may be operated under either voltage or current bias. Using a constant bias current I_b , the SQUID voltage V_{SQ} exhibits a periodic dependence on the magnetic flux threading the SQUID loop.

The mutual couplings between SQUID loop to both the feedback coil and the input coil are quantified by the mutual inductances M_{in} and M_{fb} , respectively. For the feedback coil, the mutual inductance $M_{\text{fb}} = k_{\text{fb}}\sqrt{L_{\text{fb}}L_{\text{SQ,fb}}}$, with k_{fb} denoting the geometric coupling factor, is temperature independent. In contrast, the mutual inductance $M_{\text{in}}(\lambda(T)) = k_{\text{in}}(\lambda(T))\sqrt{L_{\text{in}}L_{\text{SQ,in}}}$ is temperature dependent due to diamagnetic response of the superconducting sensing layer. Here, k_{in} denotes the geometric coupling factor that depends on the magnetic penetration depth $\lambda(T)$ of the superconducting screening layer separating the SQUID loop and the input coil. Close to the transition temperature $T_{c,\text{sens}}$, the magnetic penetration depth $\lambda(T)$ exhibits a strong temperature dependence. Consequently, a temperature change ΔT induces a change in SQUID output voltage ΔV_{SQ} according to

$$\Delta V_{\text{SQ}} = \frac{\partial V_{\text{SQ}}}{\partial T} \Delta T = \frac{\partial V_{\text{SQ}}}{\partial \Phi} \frac{\partial M_{\text{in}}}{\partial T} I_{\text{in}} \quad (1)$$

with the gain coefficient $\partial V_{\text{SQ}} / \partial T$ and I_{in} denoting the constant current running through the input coil.

To demonstrate the feasibility of the proposed microcalorimeter concept and to experimentally assess its achievable performance, we designed, fabricated, and comprehensively characterized a simple prototype MISS (see figure 2). The SQUID inductance is formed by two meander-shaped coils arranged in a first-order parallel gradiometer configuration. The superconducting sensing layer, a patterned 125 nm thick aluminum film, is sandwiched between the input coil and SQUID loop. It is electrically floating and has

no electrical contact with any other device component. Although aluminum is not an optimal choice for a practical detector with sub-eV energy resolution, due to its high transition temperature, we selected this material in order to defer the implementation of a dedicated low- $T_{c,\text{sens}}$ sensor material deposition process. For the same reasons, we omitted a particle absorber. Similar to the device reported by Krantz *et al.*¹¹, the feedback coil surrounds the SQUID loop. This configuration, however, proved to be suboptimal, as the feedback coil is also partially screened by the superconducting sensing layer, rendering the corresponding mutual inductance temperature dependent. A full functional microcalorimeter incorporating a sensing layer with 50-100 mK transition temperature, a suitable X-ray absorber, and a feedback coil geometry unaffected by the screening layer will therefore be the subject of future work. As the prototype MISS was not optimized for performance, we fabricated a second prototype device (MISSv2), in which we increased the area of the sensing layer by 33 %. As a result, the sensing layer extends beyond the SQUID loop.

We comprehensively characterized both prototype MISSs in a $^3\text{He}/^4\text{He}$ dilution refrigerator. By adjusting the operation mode of the cryostat, we swept the mixing chamber temperature between 7 mK and 1.3 K. We operated the MISS in current-bias mode using a direct-coupled high-speed dc-SQUID electronics¹³ and injected a triangular current signal with an amplitude of 1 mA into the input coil. We recorded the resulting SQUID output voltage V_{SQ} for various temperatures, and determined the mutual inductance M_{in} from the periodicity of voltage response with respect to the input current. Specifically, $M_{\text{in}} = \Delta I_{\text{in}} / v\Phi_0$, where v denotes the number of magnetic flux quanta observed over a current swing ΔI_{in} . We paid particular attention to the occurrence of hysteretic behavior. To this end, we performed three measurement cycles in which we repeatedly varied the temperature between 200 mK to 1.3 K. We varied the temperature gradually to minimize thermal gradients between the MISS and the cryostat's mixing chamber plate.

Figure 3 shows the measured temperature dependence $M_{\text{in}}(T)$ of the mutual inductance for both prototype devices. For the original MISS, three consecutive temperature cycles were performed; however, for improved visibility, only a representative selection of the data points from all cycles is shown in figure 3. Owing to limited access to the cryostat, only a single cycle was performed for MISSv2. The data from this measurement is shown with a horizontal offset of 0.25 K to improve visibility. For each device, the data sets from all cycles overlap perfectly, indicating the absence of hysteretic behavior. At temperatures $T > 1.24\text{ K}$, the sensing layer is in the normal-conducting state. Consequently, it has a negligible influence on the magnetic coupling between the SQUID loop and the input coil, and the mutual inductance approaches a value of $M_{\text{in}} = 93\text{ pH}$, which corresponds to that of an otherwise identical device without a sensing layer but with the same interlayer spacing. Below its transition temperature, the sensing layer enters the Meissner state, and strongly expels external magnetic fields. This magnetic screening leads to a pronounced reduction of the mutual inductance M_{in} , reaching near-maximum screening at temperatures below approxi-

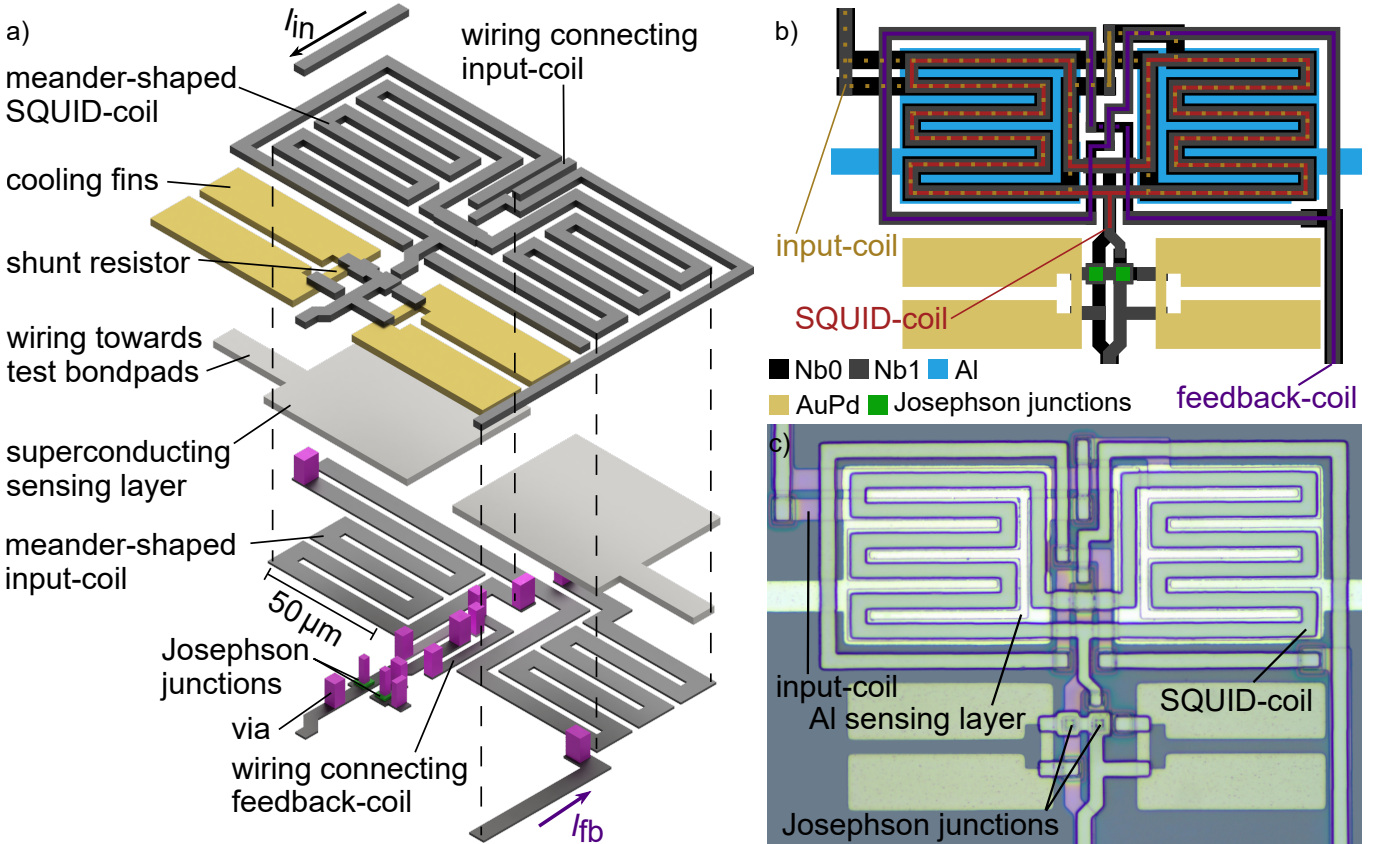


Figure 2. (a) Exploded view drawing, (b) simplified layout drawing, and (c) micrograph of the prototype Mutual Inductance Sensing SQUID (MISS). The sensing layer (silver in (a) and (c), blue in (b)), is made from Al ($T_{c,Al} \simeq 1.2$ K), while the other superconducting device components are made from Nb ($T_c \simeq 9.0$ K). In (b), the input and flux biasing coil as well as the SQUID loop are traced in yellow, purple and red, respectively.

mately 500 mK. While we expect vanishing coupling for an ideal device, i.e., $M_{in} \rightarrow 0$ for $T \rightarrow 0$, we observe a residual coupling of $M_{in} < 4$ pH even at the cryostat base temperature. Moreover, although the enlarged sensing layer of our second prototype device has little effect on the screening properties at $T > 1.1$ K, it reduces the residual coupling from 3.2 pH to 2.6 pH. The step-like features in the temperature range between 0.6 K and 0.9 K are not captured by our model, and may be attributed to local phase variations within the sensing layer, arising from inhomogeneities in film properties, temperature distribution, and/or stray magnetic fields.

To quantitatively describe our data, we used two approaches. First, we considered the decay of the magnetic field inside a superconductor due to the Meissner effect. For an infinitely large superconductor, filling the half space $x > 0$ and subjected to a magnetic field pointing in z -direction, the decrease of the z -component of the magnetic field in x -direction is given by

$$B_z(x) = B_z(0) \cdot \exp(-x/\lambda(T)), \quad (2)$$

where λ is the London penetration depth. If we consider a thin superconducting layer, for which the thickness is in the order of the penetration depth, the magnetic field exiting the superconductor is finite. Therefore, the magnetic flux

in a coil placed behind the superconducting layer is given by $\Phi(x) = \int B(x)dA$, where A is the area of the coil. Consequently, the mutual inductance between two coils that are separated by a thin superconducting layer should basically follow the dependence

$$M_1(T) = M(0) \cdot \exp(-x/\lambda(T)) \quad (3)$$

with

$$\lambda(T) = \begin{cases} \frac{\lambda_0}{\sqrt{1-(\frac{T}{T_c})^4}} & \text{for } T < T_c \\ \infty & \text{otherwise} \end{cases} \quad (4)$$

As our prototype device is based on a superconducting screening layer with finite extension, so we added a constant term $M_{off,1}$ to the fit function $M_{fit,1}(T) = M_1(T) + M_{off,1}$ to include for residual fields. The resulting fit, shown in figure 3, describes the data very well, assuming a zero-temperature London penetration depth of $\lambda_0 = \lambda(T = 0\text{ K}) \simeq 35$ nm. We attribute the slight deviation of λ_0 from the bulk value^{14–16} to the simplified nature of our model.

Our second modeling approach was initially developed for analyzing mutual inductance-based measurements of the superconducting penetration depth of thin films¹⁷. In this model,

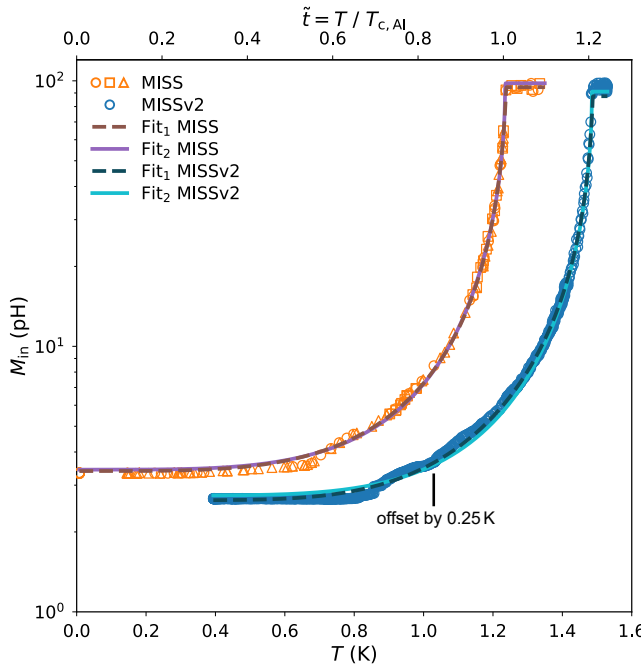


Figure 3. Measured mutual inductance M_{in} as a function of both temperature T (bottom axis) and reduced temperature $\tilde{t} = T / T_{c,\text{Al}}$ for both prototype MISS. For visibility purposes the MISSv2 data and fits have been horizontally shifted by 0.25 K and only a random sample of all data points for the original MISS are shown. For the original variant, we recorded three consecutive temperature cycles indicated by different symbols. The perfect overlap of these indicates the absence of hysteresis. The lines show fits of the measured data according to $M_{\text{fit},1}$ (dashed) and $M_{\text{fit},2}$ (dotted).

the mutual inductance of two single-turn coils with radii r_1 and r_2 , respectively, that are separated by an infinitely large, thin film of thickness d_f is described by

$$M_2(T) = \pi \mu_0 r_1 r_2 \times \int_0^{\infty} \frac{J_1(qr_1) J_1(qr_2) e^{-Dq}}{\cosh(Q(T)d_f) + \sinh(Q(T)d_f) \left[\frac{Q(T)^2 + q^2}{2Q(T)q} \right]} dq. \quad (5)$$

Here, D denotes the separation between both coils, $J_1(x)$ the Bessel function of first kind, and $Q(T)^2 = q^2 + \lambda(T)^{-2}$. As described by Claassen *et al.*¹⁷, an offset term, $M_{\text{off},2}$ is added to the model, such that $M_{\text{fit},2} = M_2(T) + M_{\text{off},2}$. For the fit, $D = 600\text{nm}$ and $d_f = 125\text{nm}$ were fixed, since they are known from profilometer measurements. The parameters r_1 and r_2 were treated as free fit parameters to include the different coil geometry, i.e., that the model expects circular coils, while our device uses meander-shaped coil. For the same reason, the offset term $M_{\text{off},2}$ was allowed to take negative values. Under these conditions, we find $\lambda_0 \simeq 180\text{nm}$, which is slightly larger than the bulk value. Overall fit describes the data of both devices very well.

At this point we want to compare the sensitivity of our MISS with that of the λ -SQUID¹⁸, a superconducting microcalorimeter that likewise exploits the temperature depen-

dence of the magnetic penetration depth of a superconductor operated close to its critical temperature. Similar to the MISS, the λ -SQUID relies on the temperature-dependent mutual inductance M_{in} between the a SQUID loop and a superconducting input coil. In contrast to the MISS, however, the λ -SQUID senses the change in penetration depth not via a separate, electrically floating sensing layer, but through a change of the effective inductance of a section of the SQUID loop caused by current redistribution. Figure 4 illustrates the substantially larger variation of the mutual inductance achieved with the MISS compared to the λ -SQUID. In addition, the MISS offer a simpler fabrication process, as the sensing layer is electrically isolated from all other circuit elements and does hence not form an integral part of the SQUID loop, avoiding, for instance, vertical interconnect accesses (vias) between different materials in the SQUID loop.

The gain coefficient $\partial V_{\text{SQ}} / \partial T$ (see equation 1 and figure 4) is an important figure of merit for assessing the performance of the MISS as a microcalorimeter. It relates a temperature change ΔT upon energy deposition to the corresponding change in the SQUID output voltage ΔV_{SQ} . From equation 1, we identify three key parameters that determine the gain coefficient: a high SQUID gain $\partial V_{\text{SQ}} / \partial \Phi$, a large temperature sensitivity of the mutual inductance $\partial M_{\text{in}} / \partial T$ and a large input current I_{in} . Increasing any of these parameters enhances the gain coefficient and, consequently, the sensitivity of the MISS. Moreover, the explicit dependence of the gain factor on the bias current I_{in} enables *in situ* tuning of the detector gain, even during event detection. This provides additional operational flexibility, for example, to optimally match the detector output to the dynamic range of digitizers in the readout chain.

To estimate of the achievable energy resolution ΔE_{FWHM} of a MISS employing a sensing layer $T_{c,\text{sens}} < 100\text{mK}$, we follow the approach introduced by Schuster *et. al.*¹⁸ for the λ -SQUID. We assume that the temperature dependence of the mutual inductance $M_{\text{in}}(\tilde{t})$ is governed solely by the reduced temperature $\tilde{t} = T / T_{c,\text{sens}}$. Accordingly,

$$\frac{\partial M}{\partial T} = \frac{\partial M}{\partial \tilde{t}} \frac{\partial \tilde{t}}{\partial T}. \quad (6)$$

This assumption is well justified, as the magnetic penetration depth of superconductors exhibits the same reduced-temperature scaling. To estimate the achievable energy resolution for low- $T_{c,\text{sens}}$ sensor materials based on our measured data (see figure 4), we analyzed the relevant noise contributions. Assuming the noise contribution of the readout electronics to be negligible by designing a proper dc-SQUID and SQUID-based preamplifier, two dominant noise sources remain: intrinsic SQUID noise $\sqrt{S_{\text{E},\text{SQ}}}$ and thermodynamic energy fluctuations $\sqrt{S_{\text{E},\text{TD}}}$ among absorber, sensor, and heat bath¹⁹. The intrinsic SQUID noise contribution is given by

$$\sqrt{S_{\text{E},\text{SQ}}} = \sqrt{S_{\text{VV}}} \left(\frac{\partial V_{\text{SQ}}}{\partial T} \frac{\partial T}{\partial E} \right)^{-1}, \quad (7)$$

where $\sqrt{S_{\text{VV}}}$ denotes the SQUID voltage noise, $\partial V_{\text{SQ}} / \partial T$ the gain coefficient (see equation 1), and $\partial T / \partial E = 1 / C_{\text{det}}$ the inverse total heat capacity of the MISS, including the particle

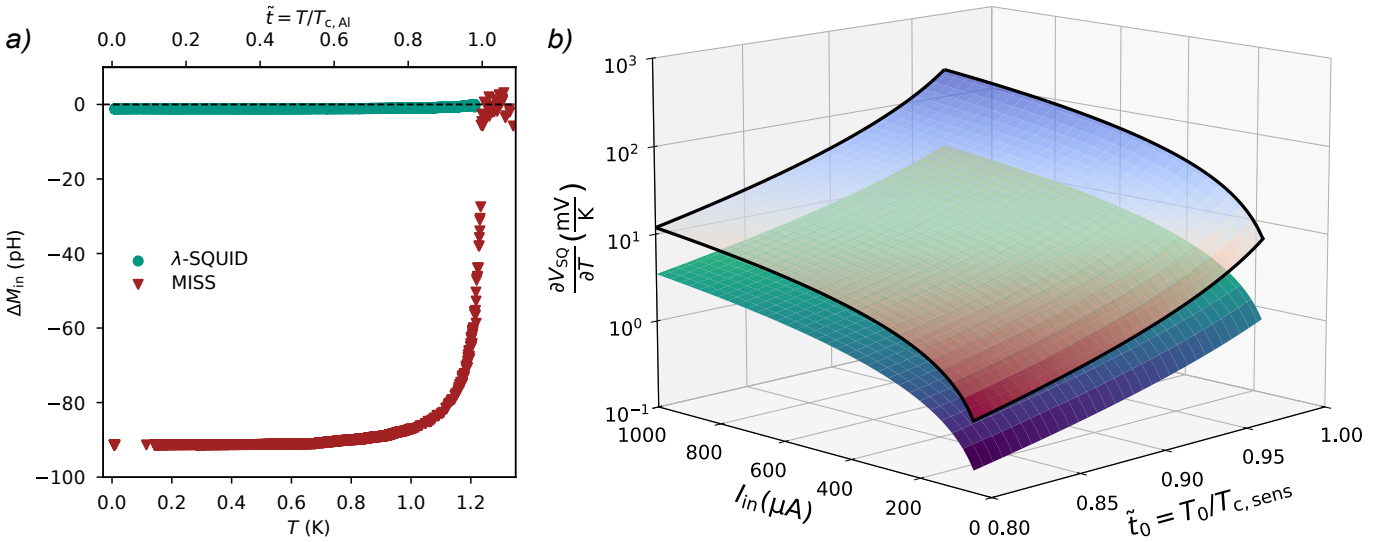


Figure 4. a) Comparison of the change in mutual inductance as function of temperature (bottom axis) and reduced temperature $\tilde{t} = T/T_{c,\text{Al}}$ for a λ -SQUID (green) and our MISS (red). The significantly larger change in mutual inductance of the MISS compared to the λ -SQUID is clearly visible. b) Comparison of the gain factor of the MISS (opaque with contour) and the λ -SQUID (colored), both calculated from the derivative of the fitted measurement data and assuming a T_c of 50 mK of the temperature-sensitive circuit element. The strong dependence on I_{in} and the operation temperature T_0 is visible as the gain factor changes over two orders of magnitude.

absorber. For an optimized SQUID²⁰, the SQUID voltage noise is $S_{\text{Vv}} = 18k_{\text{B}}TR$ and the gain coefficient can be expressed as

$$\frac{\partial V_{\text{SQ}}}{\partial T} = \frac{\partial V_{\text{SQ}}}{\partial \Phi} \frac{\partial M_{\text{in}}}{\partial \tilde{t}} \frac{I_{\text{in}}}{T_{c,\text{sens}}}. \quad (8)$$

Here, $\partial M_{\text{in}}/\partial \tilde{t}$ is obtained from fits to the data measured for our prototype devices. The contribution of thermodynamic energy fluctuations $\sqrt{S_{\text{E,TD}}}$ can be estimated using thermal properties of the detector⁷:

$$S_{\text{E,TD}} = k_{\text{B}}C_{\text{sens}}T^2 \left[\frac{4(1-\beta)\tau_0}{1+(2\pi\tau_0 f)^2} + \frac{4\beta\tau_1}{1+(2\pi\tau_1 f)^2} \right]. \quad (9)$$

Here, C_{sens} is the heat capacity of the sensor, $\beta = C_{\text{sens}}/C_{\text{det}}$ its ratio to the total heat capacity of the MISS, and τ_0 and τ_1 denote the signal rise and decay time. The latter are set by adjusting the thermal conductance between absorber, sensor and heat bath. The achievable energy resolution ΔE_{FWHM} can then readily be estimated by

$$\Delta E_{\text{FWHM}} = 2\sqrt{2\ln 2} \left[\int_0^{\infty} \frac{|p(f)|^2}{S_{\text{E,TD}}(f) + S_{\text{E,SQ}}(f)} df \right]^{-1/2} \quad (10)$$

with the detector responsivity

$$|p(f)| = \frac{2\beta\tau_1}{\sqrt{1+(2\pi\tau_0 f)^2} \sqrt{1+(2\pi\tau_1 f)^2}}. \quad (11)$$

Figure 5 compares the achievable energy resolution for both a MISS and a λ -SQUID as a function of the total heat capacity C_{det} of the detector. For this comparison, we assume

$\tau_0 = 1 \mu\text{s}$, $\tau_1 = 1 \text{ ms}$, and $\beta = 1/2$ as well as a conservative gain factor set by a small input current of $I_{\text{in}} = 500 \mu\text{A}$ and an operation temperature of $T_0 = 0.9T_{c,\text{sens}}$. In addition, we highlight three representative detectors employing the common absorber materials gold, bismuth and tin, and a benchmark absorber size of $250 \mu\text{m} \times 250 \mu\text{m}$. For each material, we choose the absorber thickness to achieve a stopping power exceeding 99.99% for soft X-ray photons. This results in a thicknesses of $5 \mu\text{m}$ for gold, $8.6 \mu\text{m}$ for bismuth and $50 \mu\text{m}$ for tin. Under otherwise identical operating conditions, the MISS clearly outperforms the λ -SQUID. For a detector employing a bismuth absorber and a sensing-layer critical temperature of $T_{c,\text{sens}} = 20 \text{ mK}$, an energy resolution well below 100 meV appears feasible. Alternatively, operation at temperatures close to 100 mK with an estimated resolution of approximately 500 meV would already constitute a significant performance benchmark. Owing to the strong inverse scaling of the SQUID noise contribution with the total detector heat capacity, reducing C_{det} drives the MISS performance increasingly close to the thermodynamic noise limit. In addition, the superconducting sensing layer is expected to exhibit a heat capacity comparable to, or lower than, that of state-of-the-art magnetic microcalorimeters¹¹. As a result, MISS detectors are particularly well suited for applications requiring exceptional energy resolution at low particle energies. Finally, we note that a MISS generally allows for two distinct modes of operation. In the first mode, the detector is operated at a temperature close to $T_{c,\text{sens}}$ and with a small input current I_{in} . In this regime, the signal is dominated by the large temperature-induced change in the mutual inductance, resulting in a high gain coefficient. At the same time, the dynamic range is limited, and the strong temperature dependence of the sensing-layer heat capacity leads to pronounced nonlinearity. Never-

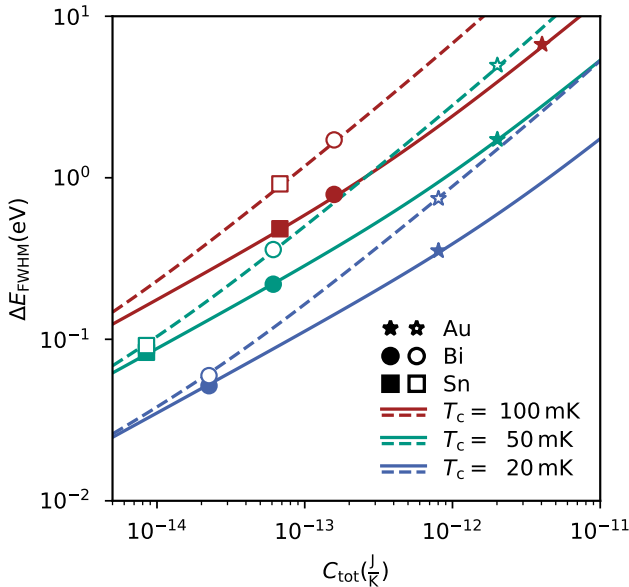


Figure 5. Estimated achievable energy resolution as a function of total heat capacity for a MISS (solid lines) and a λ -SQUID (dashed lines). Red, green and blue represent critical temperatures of 100 mK, 50 mK, and 20 mK of the temperature-sensitive circuit element. Symbols represent the achievable energy when using a $250 \mu\text{m} \times 250 \mu\text{m}$ particle absorber made of gold, bismuth, or tin whose thickness was chosen to achieve a stopping power exceeding 99.99 % for soft X-ray photons photons. filled symbols refer to a MISS, open symbols to a λ -SQUID.

theless, this mode is expected to provide the lowest achievable energy resolution, and no hysteretic behavior was observed in our measurements. The second mode corresponds to operation at temperatures significantly below $T_{c,\text{sens}}$. In this regime, the reduced temperature sensitivity of the mutual inductance $\partial M_{\text{in}} / \partial T$ can be compensated by increasing the input current I_{in} , thereby maintaining a gain coefficient comparable to that of the first mode. The maximum input current is limited by the ampacity of the input coil and the critical magnetic field of the sensing layer. A more detailed investigation of this operating mode will be the subject of future work.

In summary, we have presented a novel SQUID-based superconducting microcalorimeter whose gain can be tuned in situ. The design leverages the steep temperature dependence of the magnetic penetration depth near the superconductor's critical temperature (T_c), which in turn modulates the mutual inductance between an input coil and the SQUID loop, while allowing real-time adjustment of that input current. We have designed, fabricated, and thoroughly characterized prototype devices using an Al-based sensor layer to map out the temperature-dependent variation of mutual inductance. Importantly, we have not observed any sign for hysteresis, a common pitfall in superconducting microcalorimeter performance. Extrapolating from our data, we anticipate that, with optimized absorber and sensor materials, an energy resolution below 100 meV is within reach.

ACKNOWLEDGMENTS

We would like to thank A. Stassen for support during device fabrication. We acknowledge the financial support by the KIT Center of Elementary Particle and Astroparticle Physics (KCETA). Furthermore, C. Schuster acknowledges financial support by the Karlsruhe School of Elementary Particle and Astroparticle Physics: Science and Technology (KSETA). This work was partially funded by the Deutsche Forschungsgemeinschaft (DFG, German Research Foundation) – Projekt-nummer (project number) 467785074.

AUTHOR DECLARATIONS

Conflict of Interest

The authors have no conflicts to disclose.

Author Contributions

Jodok Zeuner: Conceptualization (equal); Formal Analysis (lead); Investigation (lead); Software (equal), Visualization (lead); Writing – original draft (lead); Writing/Review & Editing (equal). **Constantin Schuster:** Conceptualization (equal); Formal Analysis (supporting); Investigation (supporting); Software (equal); Writing/Review & Editing (equal). **Sebastian Kempf:** Conceptualization (equal); Formal Analysis (supporting); Funding Acquisition (lead); Investigation (supporting); Project Administration (lead); Resources (lead); Supervision (lead); Visualization (supporting); Writing – original draft (supporting); Writing/Review & Editing (equal).

DATA AVAILABILITY STATEMENT

The data that support the findings of this study are available from the corresponding author upon reasonable request.

REFERENCES

1. S. Friedrich, "Cryogenic X-ray detectors for synchrotron science," *J Synchrotron Radiat* **13**, 159–71 (2006).
2. J. Uhlig, W. B. Doriese, J. W. Fowler, D. S. Swetz, C. Jaye, D. A. Fischer, C. D. Reintsema, D. A. Bennett, L. R. Vale, U. Mandal, G. C. O'Neil, L. Mjaja-Avila, Y. I. Joe, A. El Nahhas, W. Fullagar, F. Parnefjord Gustafsson, V. Sundström, D. Kurunthu, G. C. Hilton, D. R. Schmidt, and J. N. Ullom, "High-resolution X-ray emission spectroscopy with transition-edge sensors: present performance and future potential," *J. Synchrotron Rad.* **22**, 766–775 (2015).
3. W. B. Doriese, K. M. Morgan, D. A. Bennett, E. V. Denison, C. P. Fitzgerald, J. W. Fowler, J. D. Gard, J. P. Hays-Wehle, G. C. Hilton, K. D. Irwin, Y. I. Joe, J. A. B. Mates, G. C. O'Neil, C. D. Reintsema, N. O. Robbins, D. R. Schmidt, D. S. Swetz, H. Tatsuno, L. R. Vale, and J. N. Ullom, "Developments in Time-Division Multiplexing of X-ray Transition-Edge Sensors," *J. Low Temp. Phys.* **184**, 389–395 (2016).
4. S. Kraft-Bermuth, D. Hengstler, P. Egelhof, C. Enss, A. Fleischmann, M. Keller, and T. Stöhlker, "Microcalorimeters for X-Ray Spectroscopy of Highly Charged Ions at Storage Rings," *Atoms* **6**, 59 (2018).

⁵G. Irwin, K.D. and Hilton, "Transition-Edge Sensors," in *Cryogenic Particle Detection*, edited by C. Enss (Springer Berlin Heidelberg, Berlin, Heidelberg, 2005) pp. 63–150.

⁶J. N. Ullom and D. A. Bennett, "Review of superconducting transition-edge sensors for x-ray and gamma-ray spectroscopy," *Supercond. Sci. Technol.* **28**, 084003 (2015).

⁷A. Fleischmann, C. Enss, and G. Seidel, "Metallic magnetic calorimeters," in *Cryogenic Particle Detection*, edited by C. Enss (Springer Berlin Heidelberg, Berlin, Heidelberg, 2005) pp. 151–216.

⁸S. R. Bandler, K. D. Irwin, D. Kelly, P. N. Nagler, J. P. Porst, H. Rotzinger, J. E. Sadleir, G. M. Seidel, S. J. Smith, and T. R. Stevenson, "Magnetically Coupled Microcalorimeters," *J. Low Temp. Phys.* **167**, 254–268 (2012).

⁹S. Kempf, A. Fleischmann, L. Gastaldo, and C. Enss, "Physics and Applications of Metallic Magnetic Calorimeters," *J. Low Temp. Phys.* **18**, 1–15 (2018).

¹⁰S. J. Lee, J. S. Adams, S. R. Bandler, J. A. Chervenak, M. E. Eckart, F. M. Finkbeiner, R. L. Kelley, C. A. Kilbourne, F. S. Porter, J. E. Sadleir, S. J. Smith, and E. J. Wassell, "Fine pitch transition-edge sensor X-ray microcalorimeters with sub-eV energy resolution at 1.5 keV," *Appl. Phys. Lett.* **107**, 223503 (2015).

¹¹M. Krantz, F. Toschi, B. Maier, G. Heine, C. Enss, and S. Kempf, "Magnetic microcalorimeter with paramagnetic temperature sensors and integrated dc-SQUID readout for high-resolution x-ray emission spectroscopy," *Appl. Phys. Lett.* **124**, 032601 (2024).

¹²F. Toschi, B. Maier, G. Heine, T. Ferber, S. Kempf, M. Klute, and B. von Krosigk, "Optimum filter-based analysis for the characterization of a high-resolution magnetic microcalorimeter," *Phys. Rev. D* **109**, 043035 (2024).

¹³D. Drung, C. Hinrichs, and H.-J. Barthelmeß, "Low-noise ultra-high-speed dc SQUID readout electronics," *Supercond. Sci. Technol.* **19**, S235 (2006).

¹⁴F. Behroozi and M. Garfunkel, "Penetration depth in superconducting aluminum as a function of magnetic field and temperature," *Physica* **55**, 649–655 (1971).

¹⁵T. E. Faber and A. B. Pippard, "The penetration depth and high-frequency resistance of superconducting aluminium," *Proc. R. Soc. Lond. A* **231**, 336–353 (1955).

¹⁶D. López-Núñez, A. Torras-Coloma, Q. Portell-Montserrat, E. Bertoldo, L. Cozzolino, G. A. Ummarino, A. Zacccone, G. Rius, M. Martínez, and P. Forn-Díaz, "Superconducting penetration depth of aluminum thin films," *Supercond. Sci. Technol.* **38**, 095004 (2025).

¹⁷J. H. Claassen, M. L. Wilson, J. M. Byers, and S. Adrian, "Optimizing the two-coil mutual inductance measurement of the superconducting penetration depth in thin films," *J. Appl. Phys.* **82**, 3028–3034 (1997).

¹⁸C. Schuster and S. Kempf, "SQUID-based superconducting microcalorimeter with in situ tunable gain," *Appl. Phys. Lett.* **123**, 252603 (2023).

¹⁹D. McCammon, "Thermal Equilibrium Calorimeters – An Introduction," in *Cryogenic Particle Detection*, edited by C. Enss (Springer Berlin Heidelberg, Berlin, Heidelberg, 2005) pp. 1–34.

²⁰C. D. Tesche and J. Clarke, "dc SQUID: Noise and optimization," *J. Low Temp. Phys.* **29**, 301–331 (1977).